Materials Science in Semiconductor Processing 40 (2015) 885–889

Contents lists available at ScienceDirect

Materials Science in Semiconductor Processing

journal homepage: www.elsevier.com/locate/mssp

Hierarchically assembled nanostructures and their photovoltaic properties

Baurzhan Ilyassov [a], Niyazbek Ibrayev [a,*], Nurxat Nuraje [b,*]

[a] Institute of Molecular Nanophotonics, E.A. Buketov Karaganda State University, 100028 Karaganda, Kazakhstan
[b] Department of Chemical Engineering, Texas Tech University, Lubbock, TX 79409, USA

ARTICLE INFO

Article history:
Received 16 May 2015
Received in revised form
29 July 2015
Accepted 29 July 2015
Available online 7 August 2015

Keywords:
Dye-sensitized solar cell
Zinc oxide nanomaterials
Photovoltaic
Photoluminescence
DSSCs
Electrochemical impedance spectroscopy

ABSTRACT

In this study, the effect of morphology and defect density of ZnO nanostructures on photovoltaic performance and electron transport properties of Dye-sensitized solar cells (DSSCs) have been investigated by using highly stable electrolytes which consist of high boiling organic solvents and a mixture of ionic liquids with relatively low viscosity. Two different ZnO nanoarrays with rod and sheet morphologies were fabricated and assembled for photovoltaic and electron transport study of the DSSCs. A photoluminescence spectra study indicated that nanosheets had more defect density compared to nanorods, which resulted in a lower open circuit photovoltage. Electrochemical impedance spectroscopy (EIS) and dye absorption amount analysis further explained the high short-circuit current density (J_{sc}) of the DSSC with ZnO nanosheet structure based on the dye-loading amount, effective electron lifetime and electron density.

1. Introduction

DSSCs based on nanostructured metal oxides have attracted great attention of researchers in the recent years [1–3]. Preparation technologies of DSSCs are much easier and cheaper than that of solar cells based on p–n junction [4]. The efficiency of DSSCs has reached a value of more than 10% [5], and the efficiency of organic–inorganic perovskite solar cells, which are also based on metal oxides, has exceeded 15% [6].

One of the key components of the DSSCs is a metal oxide semiconductor photoelectrode which performs a double function: (1) It is a scaffold with a large specific surface needed for the dye loading, and (2) at the same time it is an electron transport material [1]. Most studies focus on nanostructured TiO_2 as photoelectrode of DSSCs. The TiO_2-based DSSC has shown the highest efficiency so far.

ZnO nanostructures are alternative material as a photoelectrode of DSSC. The bandgap and the conduction band edge position of ZnO is approximately the same as that of TiO_2 [7–14]. However so far, the efficiency of DSSCs based on ZnO nanostructures is lower than one based on TiO_2. The efficiency of DSSCs based on multilayer assembly of ZnO nanowire arrays has reached 7% [15].

Several reports suggest that dye adsorption is the major problem in ZnO-based DSSCs [16–18]. DSSCs with high dye loading tend to be inefficient, whereas cells with lower dye loading show good quantum efficiencies. These problems are mainly related to the high acidity of the carboxylic acid binding groups of the dyes that can lead to dissolution of ZnO and precipitation of dye-Zn^{2+} complexes, leading to a poor overall electron injection efficiency of the dye [18].

According to Guillén et al. [19], the majority of studies regarding ZnO-based DSSCs have been focused on searching for suitable dyes for ZnO. However, in comparison with TiO_2, less detailed studies of electron transport and recombination have been carried out on DSSCs based on ZnO nanostructures.

In this paper, we studied the effect of morphology of low-dimensional ZnO nanostructures (nanorods and nanosheets) and its defect density on the photovoltaic and electron transport properties. ZnO nanorods and nanosheets were synthesized by hydrothermal and electrochemical deposition methods, respectively. Nanorods and nanosheets are nanocrystals with wurtzite crystal structure and have high specific surface. A contribution of crystal face (0001), which is a polar plane, is prevailing for nanosheets. This is the reason why these two nanostructures are of great interest as there is possibility to evaluate the influence of polar plane, defect density, and morphology of these nanostructures on photovoltaic and electron transport properties. In this work, the effect of morphology and defect density of ZnO nanostructures on

* Corresponding authors.
E-mail addresses: nurxat.nuraje@ttu.edu, niazibraev@mail.ru (N. Nuraje).

http://dx.doi.org/10.1016/j.mssp.2015.07.087
1369-8001/

photovoltaic performance and electron transport properties of DSSCs have been investigated in presence of the highly stable electrolytes (including the high boiling organic solvent and a mixture of ionic liquids with relatively low viscosity) using the following approaches: photoluminescence study, electrochemical impedance spectroscopy, analysis of dye-loading amount in the photoelectrodes in parallel with solar cell performance measurement.

2. Experimental

2.1. Preparation of ZnO nanorods

2.1.1. Preparation of ZnO seed layers

ZnO seed layers were prepared by the sol–gel spin coating fabrication process [20]. Zinc acetate dehydrate [$(Zn(CH_3COO)_2 \cdot 2H_2O$, Sigma Aldrich)] was dissolved in the mixed solution of monoethanolamine (C_2H_7NO, Sigma-Aldrich) and isopropyl alcohol. The concentrations of both zinc acetate dehydrate and monoethanolamine in the resulting solution are 0.5 M. The coating solution was spin-coated onto ITO substrates at 3000 rpm for 5 times. The ITO substrates were subsequently annealed at 400 °C in air for 30 min in order to convert zinc acetate to ZnO.

2.1.2. Hydrothermal deposition

ZnO nanorods were prepared in our lab according to hydrothermal approach. ZnO nanorods were grown by vertically placing the ZnO-seeded ITO substrates in solutions with 25 mM $Zn(NO_3)_2$ (Sigma-Aldrich) and 25 mM hexamethylenetetramine ($C_6H_{12}N_4$, Sigma-Aldrich) at 90 °C for 10 h. In order to obtain a constant nanorod array growth rate, the solutions were refreshed during the reaction period (solution turnover time 2 h). Subsequently, the substrates were washed with water/ethanol and annealed at 400 °C for 30 min to remove any residual organics.

2.2. Preparation of ZnO nanosheets

The ZnO nanosheets were fabricated by the electrochemical deposition of the arrays of hexagonal $Zn_5(OH)_8Cl_2$ nanosheets, followed by a pyrolytic transformation of $Zn_5(OH)_8Cl_2$ into ZnO nanosheets. The arrays of hexagonal $Zn_5(OH)_8Cl_2$ nanosheet were electrodeposited on ITO in the aqueous electrolyte of 0.05 M Zn $(NO_3)_2$ and 0.1 M KCl with a three-electrode electrochemical configuration. In brief, an ITO substrate, a graphite electrode, and a saturated Ag/AgCl electrode were used as the working electrode, the counter electrode, and the reference electrode, respectively. The electrodeposition was performed at −1.1 V and 50 °C for 30 min. Upon thermal treatment at 400 °C in air, the obtained $Zn_5(OH)_8Cl_2$ nanosheets were converted into ZnO nanosheets via solid-state crystal phase transformation, without altering the hexagonal sheetlike shape.

2.3. Assembly of DSSC

The ZnO-based photoanodes, each with an active surface area of 0.2 cm^2, were dyed by immersing them in a dry ethanol solution containing 0.5 mM of N719 (Solaronix) at 50 °C for 1 h. An ITO substrate coated with Pt was used as the counter electrode. Pt coat was prepared by electrodeposition methods on ITO that can be found elsewhere [21,22]. The DSSC was fabricated by placing the Pt-coated counter electrode over the dyed ZnO-based photoanode separated by a 25 μm thick thermoplastic sealing spacer (Meltonix 1170-25, Solaronix) that determines the thickness of the electrolyte layer. The internal space of cell was filled with a highly stable liquid electrolyte. It used two different electrolytes: (1)-Iodolyte Z-150 (Solaronix; Redox couple: iodide/tri-iodide; redox concentration: 150 mM; additives: ionic liquid, alkylbenzimidazole, thiocyanate; solvent: 3-methoxypropionitrile) and (2)-Mosalyte TDE-250 (Solaronix; Redox couple: Iodide/tri-iodide; redox content: iodine/ionic liquid [1/24, 160 mM]; notable additive: alkylbenzimidazoleIonic; liquid content: 1-ethyl-3-methylimidazolium iodide; 1,3-dimethylimidazolium iodide; 1-ethyl-3- methylimidazolium tetracyanoborate). Iodolyte Z-150 and Mosalyte TDE-250 further in this paper will be called *electrolyte* 1 and *electrolyte* 2, respectively. Schematic cross-sectional image of DSSC based on ZnO nanostructures is shown in Fig. 1.

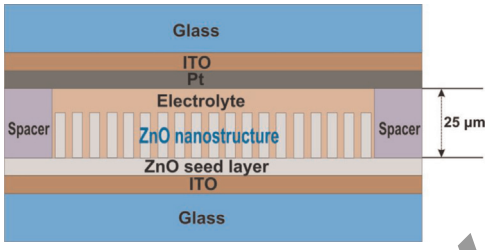

Fig. 1. Schematic cross-sectional image of DSSC based on ZnO nanostructures.

2.4. Measurements

The surface morphology of obtained nanostructures was characterized on a field-emission scanning electron microscope (FESEM MIRA-3, Tescan). The luminescence spectrum of ZnO nanostructures was measured on a highly sensitive fiber-optic spectrophotometer AvaSpec-2048 at room temperature; photoexcitation of samples was performed by the third harmonic of a neodymium laser LCS-DTL-374QT (λ=355 nm, τ=7 ns, E=5 mJ). The absorption spectrum was measured by the spectrophotometer (AvaSpec-2048) at room temperature after the dye molecules were desorbed from ZnO nanostructures in 0.1 mol/L NaOH solution of water and ethanol (50:50, v/v). The photocurrent–voltage characteristics were measured using a Source Meter instrument (Keithley 2400) by irradiating with simulated solar light, that is, AM 1.5 100 mW/cm^2 (PET Photo Emission Tech., Inc). The cell active area was 0.2 cm^2. The impedance of the cells was measured by using an impedance meter (Z-500PRO, Elins). All impedance measurements were performed under a bias light illumination of 100 mW/cm^2 from a simulated solar light (PET Photo Emission Tech., Inc) at open circuit condition. Impedance measurement of cells was recorded in a frequency range from 0.05 Hz to 200 kHz with an AC amplitude of 10 mV.

3. Result and discussion

Photovoltaic properties of the DSSC cells with nanorod and nanosheet arrays were measured and listed in Table 1. Fig. 2 shows the SEM images of nanorod and nanosheet arrays obtained by hydrothermal and electrochemical methods, respectively. Fig. 3 shows current–voltage characteristics of DSSCs consisting of the newly synthesized ZnO nanostructures and *electrolyte* 1.

As shown in Fig. 3 and Table 1, it is found that the short-circuit

Table 1
Photovoltaic performances of DSSCs consisting of the nanorod and nanosheet arrays of ZnO and with *electrolyte* 1.

	J_{SC}, mA/cm^2	V_{OC}, V	FF
DSSC based on the nanorod array	0.68	0.66	0.52
DSSC based on the nanosheet array	3.72	0.37	0.36

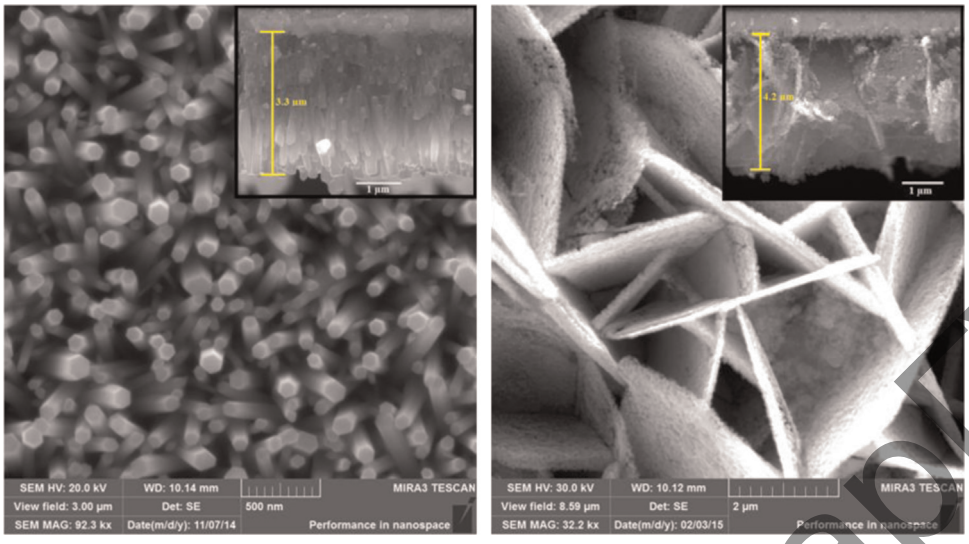

Fig. 2. SEM images of arrays of ZnO nanorod (on the left) and nanosheet (on the right). The insets are cross sectional images of nanostructures.

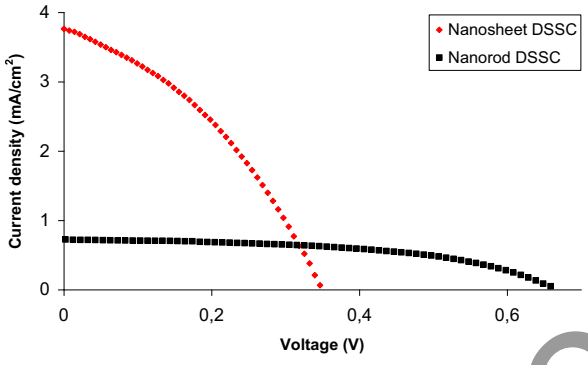

Fig. 3. Current–voltage characteristic of DSSCs based on the ZnO nanorod and nanosheet arrays.

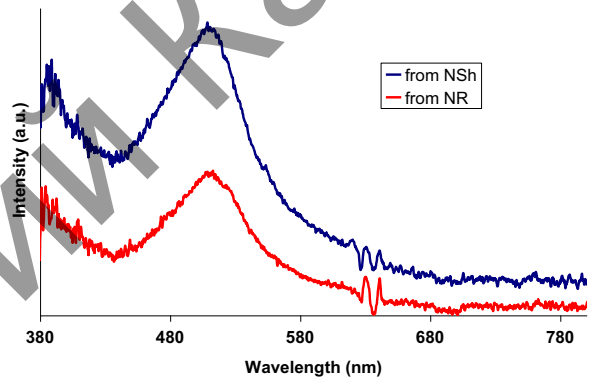

Fig. 4. UV–vis absorption spectra of dyes desorbed from ZnO nanostructures.

current density (J_{sc}) of the nanosheet array (NSh cell) cell is almost 5–6 times more than J_{sc} of the nanorod array (NR cell) -based cell. However, the open circuit voltage (V_{OC}) of NSh cell is almost two times lower than U_{oc} of NR cell and the fill factor (FF) NSh cell is significantly lower than FF of NR cell.

Since the same dye was used, the large contrast between J_{sc} of the two cells is most likely because these two structures have the different surface areas and different light scattering properties. Obviously, the nanosheet structure has a feature size comparable to the light wavelength, which may generate stronger light scattering and increase the current density, however, for determination of the influence of light scattering properties needs further investigations. However, it is also possible that photoexcited electrons inject more efficiently from the dye molecules into ZnO through the polar face of ZnO, which has the extremely large contribution to the total surface areas of the nanosheet array. As mentioned above, the poor electron injection from the dye into ZnO is the main challenge of DSSCs based on ZnO. The absorption of desorbed dye molecules in the NaOH solution is shown in the Fig. 4. It is clearly seen from the dye absorption spectrum that the dye absorption amount loaded on nanosheet array are significantly larger than that on nanorod array. This result indirectly implies that surface area of nanosheet array is larger than that of nanorod array.

A significant impact on the cell photovoltage has the defect density of the semiconductor. Defects can be electron traps and can lower the concentration of the injected electron in the conduction band of the semiconductor. The photovoltage of the cell corresponds to the increase of the quasi-Fermi level of the semiconductor, E_{Fn}, under a constant illumination with respect to the dark value, E_{F0}, which equals the electrolyte redox energy [23]. The quasi-Fermi level of the semiconductor depends on the electron concentration in the conduction band, n, and given by the following equation [23]:

$$V_{OC} = E_{Fn} - E_{F0}/e = (k_B T/e)\ln\frac{n}{n_0}$$

Here $k_B T$ is the thermal energy, e is the positive elementary charge, and n_0 is the concentration in the dark. Clearly, the trapping has a major impact on the V_{OC} generated by a constant

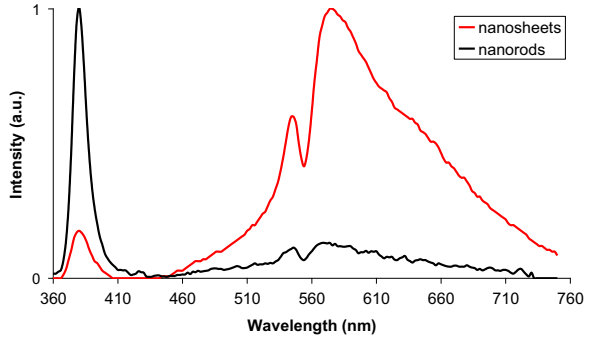

Fig. 5. The normalized PL spectra of nanosheet and nanorod arrays of ZnO. (For interpretation of the references to color in this figure, the reader is referred to the web version of this article.)

illumination. Therefore, the low value of V_{OC} of NSh in comparison with V_{OC} of NR cell may be related to the effect of defects.

The photoluminescence (PL) properties of nanosheets and nanorods have been investigated to qualitatively evaluate their crystallinity. Fig. 5 shows the PL spectra of nanosheets (red line) and nanorods (black line). For the two samples, a sharp emission peak at 380 nm and a broad band with two peaks centered at 546 nm and 576 nm were observed. The UV emission can be attributed to recombination of the free excitons or near band edge emission of the wide band-gap ZnO [23,24]. The visible light emission, relating to defects, is generally assigned to oxygen vacancies or zinc interstitials [25,26]. From comparison of the two lines, it can be observed that the black line exhibits a very strong UV emission and a negligible visible emission, while the red line shows a relatively strong visible emission. Their ratios of UV/visible emissions are 7.7 and 0.17 under our current measurement conditions, respectively. This result indicates that the nanosheets have much more defect density, or it is due to the different disorder or defects located at different crystal planes [27,28].

In the DSSCs based on TiO_2 films, the majority of the photoinjected electrons are located in trap states in the nanostructured TiO_2 film [29,30], leading to a trapped electron density that greatly exceeds the conduction electron density. These electrons must be released thermally to the conduction band before they can reach the interface and transfer to I_3^- ions. These trapping and detrapping transport models of photoinjected electrons have been confirmed by the data of electrical impedance spectroscopy (EIS), intensity-modulated photovoltage spectroscopy (IMVS) and photovoltage decay measurements [29–31].

Electrochemical impedance spectroscopy (EIS) was used to further examine the influence of morphology and a defect density of these ZnO nanostructures on electron transport properties of the cells. General transmission line model of ZnO nanostructured DSSCs, as shown on Fig. 6, based on the diffusion–recombination model proposed by Bisquert [32] is applied to analyze the electron transport properties in the cells. The Nyquist plots for impedance data of the NSh and NR cells and the fitting results are shown in Fig. 7 and Table 2 respectively. The electron transport parameters of the ZnO nanostructured cells were estimated from the Nyquist plots according to the procedure demonstrated by Adachi et al. [33]. It is shown in Table 2 that the electron densities at the steady state (n_s) in the conduction band of NSh-ZnO cell is approximately 3–4 times larger than that of NR- ZnO cell. This result implies that larger number of electrons is injected in NSh, which are consistent with high J_{SC}. Moreover, For NSh-ZnO cell, the effective electron lifetime (τ_{eff}) in NSh is higher than τ_{eff} in NR (see the inset in Fig. 5b). According to Bisquert et al. [34,35], the electron diffusion length ($L_n=(D^*\tau_{eff})^{1/2}$ is found to vary with electron density and proportional to $(\tau_{eff})^{1/2}$. The collection diffusion length, L_c, determines the short circuit current of a solar cell which is illuminated with light of near-bandgap wavelength [36,37]. Therefore, the high electron density and longer electron life time in NSh-ZnO

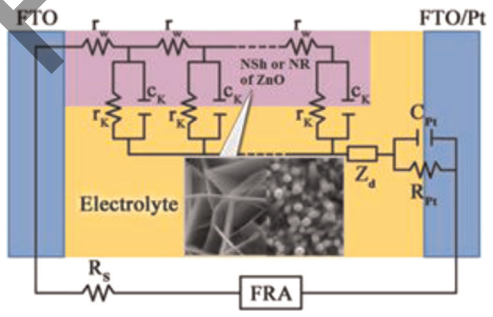

Fig. 6. General transmission line model of ZnO nanostructures-based DSSCs.

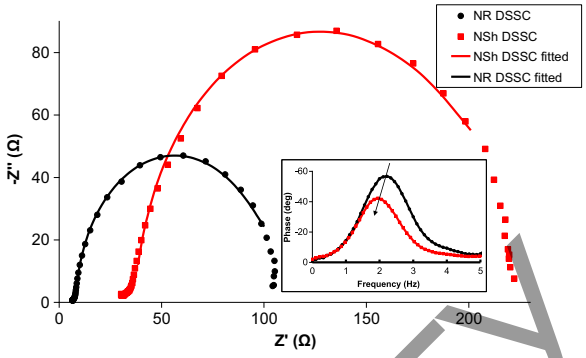

Fig. 7. Nyquist plots of DSSCs performed under illumination at the applied bias of V_{oc}. The solid lines are the fitting results from the equivalent circuit model of ZnO DSSCs. The inset is Bode phase plots.

cell are to some degree explain the high short circuit current of the cell.

Further, in our study, we used a highly stable electrolyte based on a mixture of ionic liquids with relatively low viscosity (*electrolyte* 2). Fig. 8 and Table 3 show current–voltage characteristics and photovoltaic performance of DSSC based on ZnO nanosheet array and *electrolyte* 2. For comparison, the data for DSSC based on ZnO nanosheet and *electrolyte* 1 also are shown.

As shown in Fig. 8 and Table 3, U_{OC} of the cell with the *electrolyte* 2 is virtually 1.5 times higher than that of the cell with *electrolyte* 1. On contrary, J_{SC} of the cell with *electrolyte* 2 is relatively lower than that of the cell with *electrolyte* 1. The variation of V_{OC} is either related to the recombination losses or the energy difference between conduction band edge of ZnO and the standard redox potential of I_3^-/I^- [38]. Fig. 9 shows the mid-frequency range of EIS spectra (Bode phase plots) of the NSh cell with *electrolyte* 2 (blue curve) and the NSh cell with *electrolyte* 1 (red curve). Peaks of the blue and red curves are nearly at the same frequency. This indicates that the effective electron lifetime and the recombination rate constant in cells with these different electrolytes differ insignificantly. Therefore, the difference between photovoltage of these cells is negligible due to the recombination losses and the energy difference between conduction band edge of ZnO and the standard redox potential of I_3^-/I^-, which are determined by nature of the electrolytes used.

4. Conclusion

In this study we have investigated the properties of DSSCs with ZnO nanorod and nanosheet arrays. The nanosheets have a larger defect structure than the nanorods, which was confirmed by a relatively strong visible/defect emission. DSSC short circuit current based on nanosheet has been 5–6 times larger than that based on nanorods. This result is explained by the two studies; One is the more dye loading on nanosheet arrays confirmed by UV–vis absorption spectra of desorbed dye molecules; The other is high electron density and effective life time in the NSh-ZnO cell. The effective electron lifetime in nanosheets is approximately two times larger than that in nanorods. However, we do not exclude the possibility that the electron photoinjection from the dye molecules into ZnO more effectively occurs through the ZnO polar plane (0001), which makes the dominant contribution to the surface area of the nanosheets, unlike the nanorods. The photovoltage of DSSC with the nanorod array has been almost two times more than that of the cell with nanosheet array. It can be related to the high electron trap density in nanosheet, which can lower the electron quasi-Fermi level. DSSC consisting of the nanosheet array and an electrolyte, which is made of a mixture of ionic liquids of

Table 2
Electron transport properties of ZnO nanostructures estimated by EIS analyses.

	Thickness, μm	R_w, Ω	R_k, Ω	R_k/R_w	k_{eff}, s^{-1}	τ_{eff}, μs	n_s, cm^{-3}
NSh DSSC	4.2	35	152	4.34	254	3.94	4.86×10^{16}
NR DSSC	3.3	7	85	12.14	271	3.69	1.39×10^{16}

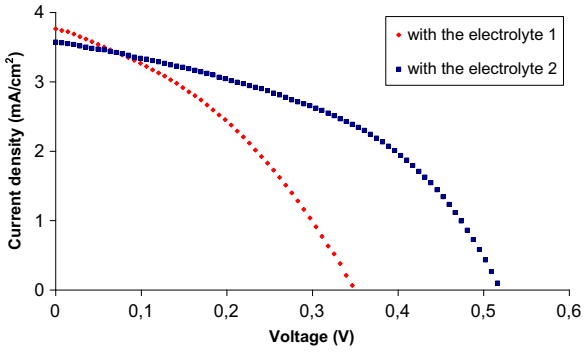

Fig. 8. Current–voltage characteristic DSSCs based on the ZnO nanosheet arrays with different electrolytes.

Table 3
Photovoltaic performance of DSSCs based on the ZnO nanosheet arrays with different electrolytes.

	J_{SC}, mA/cm²	V_{OC}, V	FF
DSSC based on ZnO nanosheet and *electrolyte* **2**	3.57	0.52	0.45
DSSC based on ZnO nanosheet and *electrolyte* **1**	3.72	0.37	0.36

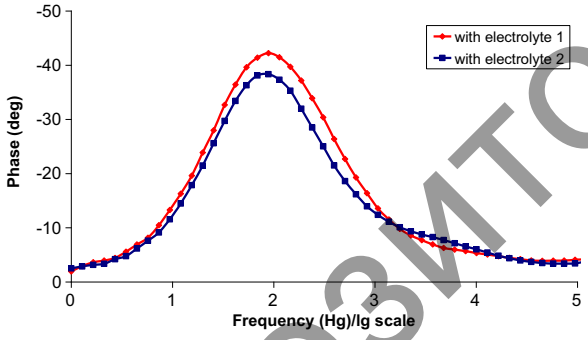

Fig. 9. Phase of EIS spectra of cell with the two different electrolytes. (For interpretation of the references to color in this figure, the reader is referred to the web version of this article.)

relatively low viscosity, has shown improved values of the photovoltage and efficiency that is explained by influence of nature of electrolytes on the energy difference between conduction band edge of ZnO and redox standard potential of the redox couples.

Acknowledgment

This work was supported by the Ministry of Education and Science of the Republic of Kazakhstan (Grant no. 535-F-15). N.N gratefully acknowledges Texas Tech University for the support of this work.

References

[1] N. Ibrayev, et al., Mater. Sci. Semiconduct. Process. 31 (2015) 358–362.
[2] N. Nuraje, R. Asmatulu, S. Kudaibergenov, Curr. Inorg. Chem. 2 (2012) 124–146.
[3] T.W. Hamann, R.A. Jensen, A.B.F. Martinson, H. Van Ryswyk, J.T. Hupp, Energy Environ. Sci. 1 (2008) 66–78.
[4] X. Sheng, et al., Opt. Commun. 314 (2013) 41–47.
[5] M. Gratzel, Nature 414 (2001) 338–344.
[6] J. Burschka, N. Pellet, S.-J. Moon, R. Humphry-Baker, P. Gao, M.K. Nazeeruddin, M. Gratzel, Nature 499 (2013) 316–319.
[7] B. Sunandan, D. Joydeep, Sci. Tech. Adv. Mater. 10 (2009) 013001.
[8] L. Znaidi, Mater. Sci. Eng.: B 174 (2010) 18–30.
[9] M. Skompska, K. Zarębska, Electrochim. Acta 127 (2014) 467–488.
[10] H. Chen, L. Zhu, H. Liu, W. Li, Thin Solid Films 534 (2013) 205–213.
[11] M. Law, L.E. Greene, J.C. Johnson, R. Saykally, P. Yang, Nat. Mater. 4 (2005) 455–459.
[12] Y. Gao, M. Nagai, T.-C. Chang, J.-J. Shyue, Cryst. Growth Des. 7 (2007) 2467–2471.
[13] E.M. Kaidashev, M. Lorenz, H. von Wenckstern, A. Rahm, H.-C. Semmelhack, K.-H. Han, G. Benndorf, C. Bundesmann, H. Hochmuth, M. Grundmann, Appl. Phys. Lett. 82 (2003) 3901–3903.
[14] E. Hendry, M. Koeberg, B. O'Regan, M. Bonn, Nano Lett. 6 (2006) 755–759.
[15] C. Xu, J. Wu, U.V. Desai, D. Gao, J. Am. Chem. Soc. 133 (2011) 8122–8125.
[16] K. Keis, J. Lindgren, S.-E. Lindquist, A. Hagfeldt, Langmuir 16 (2000) 4688–4694.
[17] C. Bauer, G. Boschloo, E. Mukhtar, A. Hagfeldt, J. Phys. Chem. B 105 (2001) 5585–5588.
[18] M. Quintana, T. Edvinsson, A. Hagfeldt, G. Boschloo, J. Phys. Chem. C 111 (2007) 1035–1041.
[19] E. Guillén, L.M. Peter, J.A. Anta, J. Phys. Chem. C 115 (2011) 22622–22632.
[20] S. Kamaruddin, K.-Y. Chan, H.-K. Yow, M. Zainizan Sahdan, H. Saim, D. Knipp, Appl. Phys. A 104 (2011) 263–268.
[21] K.S. Lee, H.K. Lee, D.H. Wang, N.-G. Park, J.Y. Lee, O.O. Park, J.H. Park, Chem. Commun. 46 (2010) 4505–4507.
[22] Y. Gao, L. Chu, M. Wu, L. Wang, W. Guo, T. Ma, J. Photochem. Photobiol. A: Chem. 245 (2012) 66–71.
[23] Y. Segawa, A. Ohtomo, M. Kawasaki, H. Koinuma, Z.K. Tang, P. Yu, G.K.L. Wong, Phys. Status Solidi (B) 202 (1997) 669–672.
[24] J.J. Wu, S.C. Liu, Adv. Mater. 14 (2002) 215–218.
[25] K. Vanheusden, C.H. Seager, W.L. Warren, D.R. Tallant, J.A. Voigt, Appl. Phys. Lett. 68 (1996) 403–405.
[26] N.O. Korsunska, L.V. Borkovska, B.M. Bulakh, L.Y. Khomenkova, V. I. Kushnirenko, I.V. Markevich, J. Lumin. 102–103 (2003) 733–736.
[27] V.M. Longo, L.S. Cavalcante, R. Erlo, V.R. Mastelaro, A.T. de Figueiredo, J. R. Sambrano, S. de Lázaro, A.Z. Freitas, L. Gomes, N.D. Vieira Jr, J.A. Varela, E. Longo, Acta Mater. 56 (2008) 2191–2202.
[28] R.C. Lima, L.R. Macario, J.W.M. Espinosa, V.M. Longo, R. Erlo, N.L. Marana, J. R. Sambrano, M.L. dos Santos, A.P. Moura, P.S. Pizani, J. Andrés, E. Longo, J. A. Varela, J. Phys. Chem. A 112 (2008) 8970–8978.
[29] R. Kern, R. Sastrawan, J. Ferber, R. Stangl, J. Luther, Electrochim. Acta 47 (2002) 4213–4225.
[30] A.B. Walker, L.M. Peter, K. Lobato, P.J. Cameron, J. Phys. Chem. B 110 (2006) 25504–25507.
[31] A. Zaban, M. Greenshtein, J. Bisquert, ChemPhysChem 4 (2003) 859–864.
[32] Q. Wang, S. Ito, M. Grätzel, F. Fabregat-Santiago, I. Mora-Seró, J. Bisquert, T. Bessho, H. Imai, J. Phys. Chem. B 110 (2006) 25210–25221.
[33] M. Adachi, M. Sakamoto, J. Jiu, Y. Ogata, S. Isoda, J. Phys. Chem. B 110 (2006) 13872–13880.
[34] J. Bisquert, F. Fabregat-Santiago, I. Mora-Seró, G. Garcia-Belmonte, S. Giménez, J. Phys. Chem. C 113 (2009) 17278–17290.
[35] J. Bisquert, M. Grätzel, Q. Wang, F. Fabregat-Santiago, J. Phys. Chem. B 110 (2006) 11284–11290.
[36] J. Bisquert, Phys. Rev. B 77 (2008) 235203.
[37] C. Schinke, D. Hinken, K. Bothe, C. Ulzhöfer, A. Milsted, J. Schmidt, R. Brendel, Energy Procedia 8 (2011) 147–152.
[38] T. Le Bahers, F. Labat, T. Pauporte, I. Ciofini, Phys. Chem. Chem. Phys. 12 (2010) 14710–14719.